THE DENSITY DEPENDENCE OF THE NUCLEAR SYMMETRY ENERGY IN HEAVY-ION COLLISIONS*

Malgorzata Zielinska-Pfabe

Smith College, Northampton, Massachusetts 01063, USA

(Received January 10, 2017)

The density dependence of the nuclear symmetry energy is of great interest over a broad range of densities from very dilute matter in supernovae up to very dense neutron stars. However, more information and stronger constraints on the symmetry energy below and above saturation density are needed. An important way to investigate the symmetry energy is to perform heavy-ion collisions. In this contribution, we give an overview of the methods to extract the symmetry energy with transport theories. We discuss the role of fluctuations in transport approaches to describe the production of light clusters and intermediate mass fragments. We discuss, in more detail, three representative examples: the equilibration of the isospin in peripheral collisions between nuclei of different asymmetry, the pre-equilibrium emission of light clusters in the compression stage of a collision, and the isospin flow at high density. We summarize with the discussion of presently known constraints and open questions about the symmetry energy with emphasizing the need of more data from heavy-ion collisions and from astrophysical observations.

DOI:10.5506/APhysPolBSupp.10.153

1. Introduction

The Equation of State (EoS) of nuclear matter has been an object of great interest for many years. The symmetry energy (SE) is the term of the strong interaction part of the EoS which arises due to an asymmetry between neutrons and protons. It is crucial to realize that the symmetry and Coulomb energies are critical for the structure of any asymmetric nuclear system: from stable and exotic nuclei to astrophysical objects. Therefore, one is interested in the symmetry energy (SE) in a large range of density from dilute systems, as in supernovae, up to very dense matter in neutron stars. Very asymmetric nuclear matter can be studied by observing astrophysical objects, especially supernovae and neutron stars. However, a stellar event is not observed

* Presented at the XXIII Nuclear Physics Workshop "Marie and Pierre Curie", Kazimierz Dolny, Poland, September 27–October 2, 2016.

frequently. In the laboratory, the nuclear EoS can be studied by performing heavy-ion collisions (HIC). These allow to choose within limits the nuclear density reached and the isotopic composition. On the other hand, HICs are non-equilibrium processes, which require a complex interpretation with the help of transport theories.

In this contribution, we want to give a compact overview of the methods of interpretation of HICs by transport theories and examples of the results, in particular, with respect to the symmetry energy (SE). For recent more extensive reviews, see *e.g.* Refs. [1, 2]. We will first define the nuclear EoS and the SE, and discuss why the latter is important. Then we will explain why to study the EoS in HICs and the methods to describe these collisions as non-equilibrium processes, namely transport theories. We will then discuss the role of fluctuations and their importance for fragmentation. We will then give some examples of investigations of the SE at low and high density (respectively incident energy). Finally, we will review the present status of knowledge of the SE and end with a summary.

2. Investigating the nuclear symmetry energy

2.1. Symmetry energy definitions and parametrizations

The nuclear SE is defined by the expansion of the binding energy per nucleon in infinite nuclear matter in terms of asymmetry $\beta = (\rho_n - \rho_p)/\rho$ as

$$E(\rho, \beta) = E_{\rm nm}(\rho) + E_{\rm sym}(\rho)\beta^2 + O\left(\beta^4\right) , \tag{1}$$

where $E_{\rm nm}$ is the energy of symmetric nuclear matter and $E_{\rm sym}$ the density-dependent symmetry energy due to strong interactions. If higher order terms in β^2 can be neglected, the SE can also be written as $E_{\rm sym}(\rho) = E(\rho, 1) - E(\rho, 0)$, *i.e.* as the difference of the energy of pure neutron matter and the energy of symmetric nuclear matter.

Around saturation density, two parametrizations of the SE are commonly employed

$$E_{\rm sym}(\rho) = S + \frac{L}{3}\left(\frac{\rho - \rho_0}{\rho_0}\right) + \frac{K_{\rm sym}}{18}\left(\frac{\rho - \rho_0}{\rho_0}\right)^2 + ... \tag{2}$$

with the symmetry value S, the slope L and the incompressibility $K_{\rm sym}$ at saturation, and alternatively as

$$E_{\rm sym}(\rho) = E^{\rm kin}_{\rm sym}(\rho) + E^{\rm pot}_{\rm sym}(\rho) = \frac{1}{3}\epsilon_{\rm F}(\rho - \rho_0)^{2/3} + C\left(\frac{\rho}{\rho_0}\right)^{\gamma} \tag{3}$$

with a symmetry kinetic term from the Fermi gas and symmetry potential term as a power law with exponent γ. L (or γ) describes how the SE changes

with density; *e.g.* for a stiff SE, L is large or $\gamma > 1$. Often the terms asy-stiff, resp. asy-soft, SE are used. Skyrme interactions allow realistic choices of the density dependence of the SE and also of a momentum dependence, which can be expressed by effective masses, especially important at high energies.

The SE is relevant over a large range of densities in nuclear and astrophysical systems. At very low density, cluster correlations depending on the asymmetry of the system are important in the neutrino-sphere of core-collapse supernovae [3]. In heavy-ion collisions in the Fermi energy regime multi-fragmentation occurs, and isospin fractionation and transport determine the isospin contents of the fragments and clusters [4]. Around saturation density, the SE determines nuclear structures in stable and exotic nuclei, *e.g.* masses, neutron skins, and collective phenomena, see *e.g.* the corresponding articles in Ref. [2]. Here, mainly the slope L of the SE at saturation is studied. The mechanism and evolution of core-collapse supernovae depend on the SE for broad range of densities and temperatures [5]. The structure of neutron stars, in particular the mass–radius relation, depends sensitively on the SE at high densities. This can also be studied in the laboratory at relativistic heavy-ion collisions [1].

The nuclear EoS and the nuclear SE can be and have been calculated in realistic many-body approaches, as discussed in this conference. A sample of calculations for symmetric and pure neutron matter is shown in the left panel of Fig. 1 for different modern many-body approaches [6]. For symmetric nuclear matter, the theories agree rather well below saturation. Above saturation they diverge, but from HICs (flow and kaon production) the symmetric EoS has been determined quite well to be rather soft. The neutron EoS, however, is less convergent, also below saturation. The difference between the two is the symmetry energy, shown in the right panel of Fig. 1. A large uncertainty is seen, particularly above saturation density. In addition, there is the momentum dependence of the symmetry potential, as it is well-known from the optical potential. The momentum dependence can be expressed in terms of an effective mass, which leads to a difference of the neutron and proton effective masses (effective mass splitting) [7]. The symmetry potential (or Lane potential) is the difference between neutron and proton potentials. It also shows large divergences between theories and a not very strong constraint from experimental data [8]. Thus, also the effective mass splitting is an issue in the determination of the SE.

Due to these uncertainties of the many-body calculations, which in a deeper analysis are seen to originate from the not well-known short-range behavior of the isovector interaction [9], one attempts to obtain constraints from nuclear structure (around saturation), from HICs, and from neutron star observations.

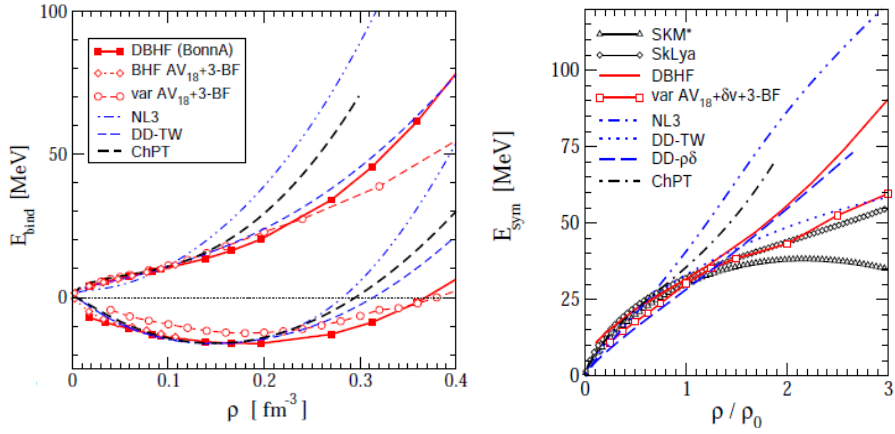

Fig. 1. (Color online) Left panel: The binding energy per nucleon for symmetric nuclear matter (lower group of curves) and pure neutron matter (upper curves) as a function of normalized density for different microscopic many-body models, which are identified in the legend. Right panel: The symmetry energy as a function of density as the difference between symmetric and pure neutron matter, again, for different microscopic many-body models. From Ref. [6].

2.2. Models of transport theory

The best way to investigate $E_{\rm sym}(\rho)$ in the laboratory is using HICs. However, the EoS and the SE are concepts of equilibrium, while HICs are dynamical processes. To deal with these, one has to use transport theories, which describe the time evolution of 1-body phase space distribution function $f(r,p;t)$ under the action of a mean-field potential $U(r,p)$, possibly momentum-dependent, and in-medium two-body collisions. The aim is a microscopic description of nucleus–nucleus collisions. The main ingredients are individual NN collisions (Cascade model) and a self-consistent mean field (Vlasov equation). Both considered simultaneously lead to the Boltzmann equation and variants of it. The main comprehensive reference to transport models is still the article by Bertsch and Das Gupta [10].

To describe the mean-field evolution, we start from the TDHF approach and introduce the single particle density $\rho(r_1,r_2)$ which obeys the TDHF equation $\partial_t\rho = -i[h,\rho]$. To obtain semi-classical equations of motion, one performs a Wigner transform of the single particle density, yielding the above 1-body distribution function $f(r,p;t)$, and then uses the gradient approximation in keeping only the lowest order term of the Wigner transform of a product. Thus we obtain the Vlasov equation, known from classical kinetic theory, *e.g.* [11]

$$\left(\frac{\partial}{\partial t} + \frac{p}{m}\nabla_r - \nabla_r U(r)\nabla_p\right) f(r,p;t) = 0\,. \tag{4}$$

For a realistic description of HICs, one has to include 2-body dissipation due to NN collisions, *i.e.* a Boltzmann collision term. It guarantees the conservation of momentum and energy, and includes Pauli blocking factors $\bar{f} := (1 - f)$ to respect the fermionic nature of the system. This leads to the Boltzmann–Uehling–Uhlenbeck (BUU) or Boltzmann–Nordheim collision term [10]

$$I_{\text{coll}} = \int \mathrm{d}v_2 \mathrm{d}v_{1'} \mathrm{d}v_{2'} |v_2 - v_1| \sigma(\Omega) (2\pi)^3 \delta(p_1 + p_2 - p_{1'} - p_{2'}) \times \left[f_{1'} f_{2'} \bar{f}_1 \bar{f}_2 - f_1 f_2 \bar{f}_{1'} \bar{f}_{2'} \right] , \tag{5}$$

where $\sigma(\Omega)$ is the total NN cross section (in medium). The collision term replaces zero on the r.h.s. of Eq. (4) to obtain the BUU equation. As a physical input, the BUU equation contains the self consistent mean-field potential U and the in-medium NN cross section.

An alternative transport equation is Quantum Molecular Dynamics, which formulates the evolution in terms of nucleon coordinates (like in classical molecular dynamics) with finite size wavepackets (QMD) [12], in contrast to the single particle density as in BUU. It can also be derived from TDHF.

The BUU transport equation is a non-linear integral-differential equation. For low dimensional model systems, a solution on a lattice has been used. For realistic HICs, it is common to introduce a test particle (TP) representation of the distribution function

$$f(r, p; t) = \frac{1}{N_{\text{TP}}} \sum_{i=1}^{AN_{\text{TP}}} \delta(r - r_i(t)) \delta(p - p_i(t)) , \tag{6}$$

where $\{r_i(t), p_i(t)\}$ are the positions and momenta of the test particles, and N_{TP} is the number of TP per nucleon [10]. For a smoother representation, also finite size TPs have been used. When introducing Eq. (6) into the Vlasov equation, one obtains Hamiltonian equations of motion for the TP centers and momenta. The collision term is simulated stochastically like in a Cascade calculation [10]. In the limit $N_{\text{TP}} \to \infty$, one obtains an exact solution of the BUU equation, which does not contain fluctuations. Extensions to include fluctuations are discussed next.

2.3. Fluctuations in transport theories

In Fig. 2, a schematic view of the production of clusters and fragments in a HIC at Fermi energies is shown. The colliding system undergoes compression with pre-equilibrium emission of light clusters. The following expansion yields primary excited intermediate mass fragments (IMFs). The secondary decay of these is usually treated in statistical models. Thus, light clusters

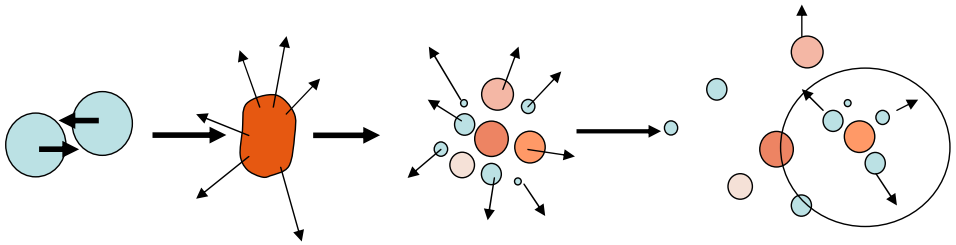

Fig. 2. Schematic picture of the production of clusters and fragments in a HIC at Fermi energies. From left to right: (1) approach phase; (2) maximum compression, pre-equilibrium emission of nucleons and light clusters; (3) primary excited IMFs and light clusters at freeze-out; (4) statistical decay of primary fragments.

and fragments are ubiquitous in HICs. It is seen in experimental data from the INDRA and FOPI collaborations of the partitioning of protons in collisions at 50 and 250 MeV/A. At 50 MeV, about 70% of the protons appear not as free protons but in clusters or larger fragments, and still 50% at the higher energy [13]. Many of these are produced dynamically during the evolution, and not only by statistical decay of the primary fragments. Thus, it is important to describe cluster and fragments production in transport theories.

Nuclear matter has regions of spinodal instabilities. After the initial compression, the expansion may bring the system below the critical density. Then fluctuations will be amplified by the mean field. When the interaction time is of the order of growth rates of instabilities, fragments will form (multi-fragmentation). Thus, fluctuations are the seeds to the formation of fragments, and similarly few-body correlations are the seeds to the formation of light clusters. However, BUU does not have correlations (mean field) and fluctuations, except numerical fluctuations due to the stochastic evaluation of the collision term. Physical fluctuations and correlations have to be introduced into the transport theory.

This is done *e.g.* in the Stochastic Mean Field method [14]. As the colliding system starts to expand, the fluctuations are introduced in coordinate space in a statistically consistent way. The variance of fluctuations is determined by assuming a Fermi gas at local thermal equilibrium

$$\sigma_{\mathrm{F}}^2 = \frac{16\pi m\sqrt{2m}}{Vh^3}\sqrt{\epsilon_{\mathrm{F}}}T\left[1 - \frac{\pi^2 T^2}{12\epsilon_{\mathrm{F}}^2} + ...\right]. \tag{7}$$

T is the local temperature determined from the kinetic energy density, ϵ_{F} the local Fermi energy depending on density, V the cell volume. In each cell, a random change of density is made in agreement with the variance given by Eq. (7), conserving mass, energy and momentum. Then we apply the

BUU procedure again to follow the evolution of the system. This method is an approximation to the Boltzmann theory with fluctuations, the so-called Boltzmann–Langevin equation.

3. Examples of isospin sensitive observables in HICs

In the following, we will give a few typical examples of observables, from which one may gain information on the SE, which rely on differences of the neutron/proton ratio during different stages of the evolution. The difference between neutron and proton currents can be approximately expressed in the following way [4]

$$j_n - j_p \approx E_{\mathrm{sym}}(\rho)\nabla I + \frac{\partial}{\partial\rho} I \nabla\rho \,. \tag{8}$$

Thus, it is driven by two effects: by isospin gradients with a strength proportional to the value of the SE ("diffusion"), and by density gradients proportional to the slope of the SE ("drift"). Our first example is the equilibration of isospin in collisions of nuclei with different asymmetry; the second the ratio of isospin partners in the pre-equilibrium emission of nucleons and light clusters, and finally the momentum distribution of the emitted nucleons, the so-called flow.

3.1. Isospin equilibration

Here, we discuss the equilibration of isospin in peripheral collisions between nuclei of different asymmetry, in this case for experiments at MSU of n-rich and n-poor isotopes of tin, ^{124}Sn and ^{112}Sn, at 50 MeV/A [15]. Quantitatively, the amount of equilibration is measured by the isospin transport (or Rami) ratio $R = (2\beta_{AB} - (\beta_{AA} + \beta_{BB}))/(\beta_{AA} - \beta_{BB})$. β_{AB} is an isospin-sensitive observable in the reaction between nuclei A and B (here, $A = {}^{124}$Sn and $B = {}^{112}$Sn). The observable used here is $\beta = N/Z$, the charge ratio of the residues in the projectile or target velocity region in mixed and symmetric reactions. The ratio is zero for complete mixing and +1 for complete transparency. The isospin transport is driven by the isospin gradient (diffusion), and is proportional to the value of the SE, which at densities below saturation is larger for an asy-soft SE. Thus, more mixing and a smaller R are expected for an asy-soft SE and *vice versa*. Figure 3 shows two calculations of this ratio compared to the experimental value of MSU. Compared are calculations with BUU [16] and a version of QMD [17] as a function of impact parameter. Both calculations fulfill the expectation that an asy-stiff SE leads a larger ratio (more so if the interaction is also momentum-dependent), which is more in agreement with the experiment. However, the value and the dependence on impact parameter differ. The results show that this ratio is sensitive to the stiffness and momentum dependence of the SE, but also to details of the model.

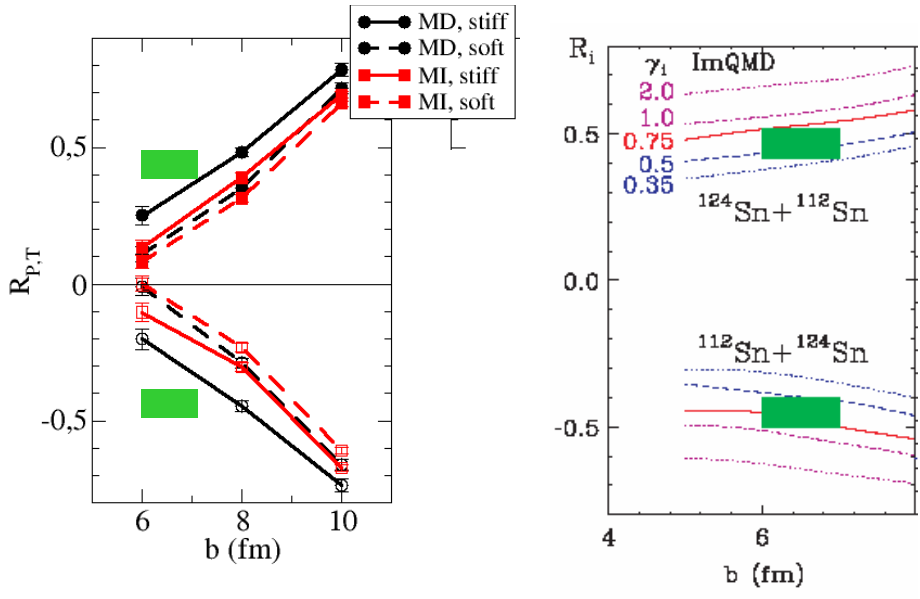

Fig. 3. (Color online) The transport ratio describing the isospin equilibration in a HIC between Sn nuclei at 50 AMeV of different asymmetry (see the text). Left panel: Calculations with the BUU-type code SMF for a stiff and a soft SE, and with (MD) and without (MI) momentum dependence [16]. Right panel: ImQMD calculations [17] also with different asy-stiffness with different exponents γ_i. The gray/green boxes represent the experimental value for this system [15].

3.2. Pre-equilibrium emission of light clusters

The second example is the pre-equilibrium emission of light clusters during the compression stage of a collision. A characteristic observable is the ratio of emitted neutrons to protons, as shown in Fig. 4 (left panel) for the reaction ^{136}Xe+^{124}Sn at 150 MeV/A as a function of the transverse energy of the emitted particle [18]. Higher transverse energies correspond to emission from earlier phases of the collision. We show results of four calculations, where the density dependence is varied from asy-soft to asy-stiff and the effective mass from $m^*_n > m^*_p$ to $m^*_n < m^*_p$. The asy-soft SE is more repulsive for neutrons and increases the ratio for low energies, while a smaller effective mass facilitates the emission, which is the dominant mechanism at higher emission energy. The possibility to disentangle the density and momentum dependence in the energy dependence of this ratio is nicely seen in the figure. The effects are similar for the ratio of isospin partners of heavier clusters as shown for the t to ^{3}He ratio in the right panel of Fig. 4. Since experimentally the efficiencies for neutrons and protons are very different,

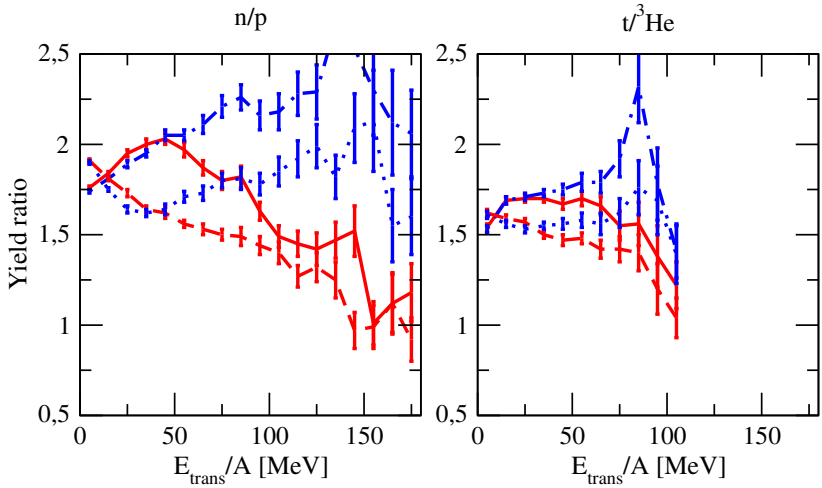

Fig. 4. (Color online) Left panel: Ratio of free neutron to proton yields in the reaction ^{136}Xe+^{124}Sn at 150 AMeV as a function of transverse energy. Shown are four calculations with different asy-stiffness and different effective mass splitting: asy-soft, $m_n^* > m_p^*$ (solid line (red)), $m_n^* < m_p^*$ (dash-dotted line (blue)); asy-stiff, $m_n^* > m_p^*$ (dashed line (red)), $m_n^* < m_p^*$ (dotted line (blue)). Right panel: The same for the ratio of triton to ^{3}He. From Ref. [18].

one likes to form a so-called double ratio for two different systems, to cancel out these efficiency differences. This has recently been measured at MSU and compared with QMD calculations [19,20]. It was shown that this double ratio is particularly sensitive to the effective masses. The data seem to favor an interaction where the effective neutron mass is smaller than the proton one. It is seen that these cluster ratios are promising observables which need to be investigated more systematically.

3.3. Isospin flow

To investigate the SE at high density, the nucleon momentum distribution is an appropriate observable, since it directly reflects the nucleon potentials. It is analyzed in terms of a Fourier series of the momentum distribution $N(\Theta, y, p_t) = N_0(v_1 \cos(\Theta) + v_2 \cos(2\Theta) + \ldots)$ as a function of the azimuthal angle Θ for fixed rapidity y and transverse momentum p_t. The first two coefficients are called directed and elliptic flow. The elliptic flow measuring the squeeze-out perpendicular to the reaction plane is determined mainly by the high density zone. The ratio of neutron-to-proton (actually $Z = 1$) flow was recently remeasured by the ASY-EOS Collaboration [21]. In an analysis with an SE in terms of the power-law exponent γ, a value of $\gamma = 0.76 \pm 0.12$ was determined, corresponding to a moderately stiff SE.

4. Conclusions and summary

The present constraints on the nuclear SE from nuclear structure and HICs are summarized in Fig. 5. Around saturation one sees the constraints from mass fits, isobaric analog states (see [22]; area with dotted boundary), and heavy-ion collisions in the Fermi energy regime (as discussed above [23, 24]; light gray area around $\rho/\rho_0 \approx 0.5$). The results in this region are seen to converge well. At very low density, a finite SE as a result of clustering of low-density matter is indicated [3]. For densities above saturation, the results from the nucleon flow measurements, discussed in the last section, are shown as the dark gray (red) region, while the light gray (yellow) region is the result of an earlier measurement of the flow. Another sensitive observable not discussed here is the pion ratio π^+/π^-, driven by the asymmetry of the matter where the pions are produced, determined by the symmetry potential. One of the results from the pion ratios is shown as the thick black/blue line, which deviates very much from the flow result [25]. However, there are also other analyses with other conclusions. A new experiment with more detailed data on the pion ratios is discussed in [23].

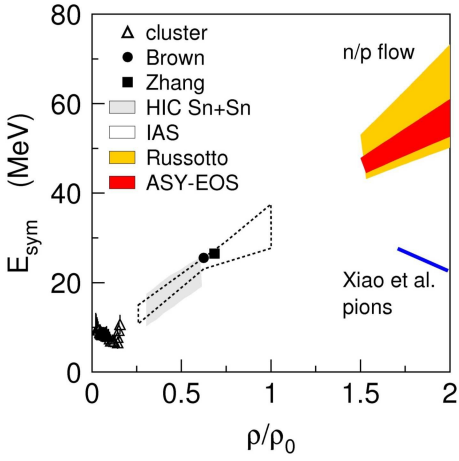

Fig. 5. (Color online) Summary of constraints on the density-dependent symmetry energy from the analysis of different data, as identified in the legend and discussed in the text. From Ref. [21].

To summarize, the Equation of State of nuclear matter, and particularly the symmetry energy interesting itself and also an important input for astrophysics in the description of core collapse supernovae, neutron star structure, and nucleosynthesis. The EoS is investigated in the laboratory in heavy-ion collisions, and interpreted with the help of complex transport models. Open problems are the treatment of fluctuations and correlations to

account for cluster and fragment production, the treatment of instable particles (*e.g.* the Δ resonance), and the consistency of transport approaches, which is presently investigated in a Code comparison project [26].

The EoS of symmetric nuclear matter ($\rho_n = \rho_p$) is fairly well-determined by now. The symmetry energy (SE) is much less constrained, and an area of very active investigations experimentally (new facilities) and theoretically. The present status can be roughly summarized as follows:

(1) constraints around and below ρ_0 begin to converge,

(2) clustering effects lead to a finite SE at very low densities,

(3) few experiments are available for high densities, but new ones are forthcoming.

The high density SE is presently the biggest uncertainty.

This review article is based on the work done together with Maria Colonna, Massimo Di Toro, LNS, INFN, Catania, Italy, Joseph Rizzo and Salvatore Maccarone (formerly LNS), Piotr Decowski, Smith College, Northampton, USA (unfortunately, recently deceased), and Hermann Wolter, University of Munich, Germany, but using results also from other workers in the field. I want to deeply thank my collaborators and, in particular, H.W. for the help with this contribution.

REFERENCES

[1] C.J. Horowitz *et al.*, *J. Phys. G* **41**, 093001 (2014).
[2] B-.A. Li *et al.*, *Eur. Phys. J. A* **50**, 9 (2014).
[3] J.B. Natowitz *et al.*, *Phys. Rev. Lett.* **104**, 202501 (2010).
[4] V. Baran *et al.*, *Phys. Rep.* **410**, 335 (2005).
[5] A.W. Steiner *et al.*, *Phys. Rep.* **411**, 325 (2005).
[6] C. Fuchs, H.H. Wolter, *Eur. Phys. J. A* **30**, 5 (2006).
[7] J. Rizzo, M. Colonna, M. Di Toro, *Phys. Rev. C* **72**, 064609 (2005).
[8] B.-A. Li, X. Han, *Phys. Lett. B* **727**, 276 (2013).
[9] O. Hen *et al.*, *Phys. Rev. C* **91**, 025803 (2015).
[10] G.F. Bertsch, S. Das Gupta, *Phys. Rep.* **160**, 189 (1988).
[11] L. Reichl, *A Modern Course in Statistical Physics*, 4$^{\text{th}}$ Edition, Wiley, 2016.
[12] J. Aichelin, *Phys. Rep.* **202**, 233 (1991).
[13] S. Hudan *et al.*, *Phys. Rev. C* **67**, 064613 (2003); W. Reisdorf *et al.*, *Nucl. Phys. A* **848**, 366 (2010).

[14] M. Colonna *et al.*, *Nucl. Phys. A* **642**, 449 (1998).
[15] M.B. Tsang *et al.*, *Phys. Rev. Lett.* **92**, 062701 (2004).
[16] J. Rizzo *et al.*, *Nucl. Phys. A* **806**, 79 (2008).
[17] M.B. Tsang *et al.*, *Phys. Rev. Lett.* **102**, 122701 (2009).
[18] H.H. Wolter *et al.*, *EPJ Web Confs.* **66**, 03097 (2014).
[19] Y.X. Zhang *et al.*, *Phys. Lett. B* **732**, 186 (2014).
[20] D.D.S. Coupland *et al.*, *Phys. Rev. C* **94**, 011601 (2016).
[21] P. Russotto *et al.*, *Phys. Rev. C* **94**, 034608 (2016).
[22] P. Danielewicz, talk given at the XXIII Nuclear Physics Workshop "Marie and Pierre Curie", Kazimierz Dolny, Poland, September 27–October 2, 2016, not submitted to the proceedings.
[23] M.B. Tsang, talk given at the XXIII Nuclear Physics Workshop "Marie and Pierre Curie", Kazimierz Dolny, Poland, September 27–October 2, 2016, not submitted to the proceedings.
[24] Z. Xiao, talk given at the XXIII Nuclear Physics Workshop "Marie and Pierre Curie", Kazimierz Dolny, Poland, September 27–October 2, 2016, not submitted to the proceedings.
[25] Z. Xiao *et al.*, *Phys. Rev. Lett.* **102**, 062502 (2009).
[26] J. Xu *et al.*, *Phys. Rev. C* **93**, 044609 (2016).